Critical Evaluation of the Use of 3D Carbon Networks Enhancing the Long-Term Stability of Lithium Metal Anodes

Xinwei Dou [1,2], Markus S. Ding [1,2], Guk-Tae Kim [1,2], Xinpei Gao [1,2], Dominic Bresser [1,2]* and Stefano Passerini [1,2]*

[1] Helmholtz Institute Ulm, Ulm, Germany, [2] Karlsruhe Institute of Technology, Karlsruhe, Germany

The lithium metal anode is considered the ultimate goal for pushing the energy density of lithium batteries to the theoretical maximum. "Coating" metallic lithium with protective (carbon) layers has been reported as a viable method to mitigate detrimental issues such as the dendritic lithium deposition and the continuous fracturing of the SEI layer. Herein, we propose a rather simple and economically efficient method employing carbonized filter paper positioned over the lithium metal electrode. After an initial spontaneous lithiation of the paper-derived 3D carbon network, lithium plating/stripping experiments reveal highly stable and rather low overpotentials—particularly when replacing the standard organic carbonate based electrolyte by ionic liquids. The final volumetric energy density of this and the many comparable approaches so far reported in literature, however, remains to be carefully considered, as illustrated by a rather quick calculation.

Keywords: lithium metal, carbon paper, ionic liquids, anode, battery

INTRODUCTION

Lithium metal is considered the "holy grail" of the anode materials for lithium batteries, actually essential to enable future battery technologies like Li-S and Li-air. Its outstanding theoretical capacity (3,860 mAh g^{-1} or 2,061 mAh cm^{-3}) and extremely low redox potential (-3.04 V vs. a standard hydrogen electrode) render it, indeed, the ultimate goal for realizing high-energy lithium batteries—independent of the chosen cathode. However, two main challenges prevent lithium metal anodes from commercialization. The safety hazards due to the potential formation of dendrites, eventually short-circuiting the cell, is certainly the most important. Nonetheless, the comparably short cycle life due to the continuous electrolyte composition and loss of electrochemically active lithium is also a performance limiting factor (Kim et al., 2013; Xu et al., 2014; Lin et al., 2017; Wood et al., 2017). Actually, this latter is also related to the dendritic lithium morphology evolving upon cycling, which increases the electrode surface area amplifying the irreversible reaction occurring at the electrode/electrolyte interface. To suppress such uneven (dendritic) lithium deposition, most attempts so far focused on improving the stability and uniformity of the solid electrolyte interphase (SEI) layer formed on the lithium metal surface by incorporating functional electrolyte additives (Xu, 2004; Xu et al., 2014; Wood et al., 2017). However, as lithium is thermodynamically unstable in the most commonly used electrolytes, the passivation of the lithium metal anode via the formation of a suitable SEI is extremely difficult to achieve (Aurbach et al., 2002). For such a reason, artificial SEI layers, such as *ex situ* formed

polymers, are attracting great interest to suppress dendrite growth (Li et al., 2016; Ding et al., 2017; Gao et al., 2017). Unfortunately, this approach eventually faces the same issues as the additive-modified SEI, i.e., the continuously changing structure and morphology of the lithium metal anode, especially at high current densities.

To address this issue, several studies have recently focused on increasing the electroactive surface area via the use of conductive 3D carbon networks, serving simultaneously as current collector and, somehow, protective layers (Yang et al., 2015; Zhang et al., 2016; Li et al., 2017; Liu et al., 2017, 2018; Lu et al., 2018; Wu et al., 2018). At first glance, one may expect that this approach should lead to fast short-circuiting, as lithium dendrites are expected to grow rapidly on the rough, but electronically conductive carbon surface. However, several research groups displayed stable long-term cycling, claiming this approach as truly beneficial for the long-term cycling stability of the lithium metal anode, while simultaneously allowing for reduced polarization issues (Yang et al., 2015; Zhang et al., 2016; Li et al., 2017; Liu et al., 2017, 2018; Lu et al., 2018; Wu et al., 2018).

Following this work, we employed an easily scalable approach for the realization of a free-standing 3D carbon network (CNW) to support lithium metal deposition, simply carbonizing filter paper under inert conditions.

MATERIALS AND METHODS

3D Carbon Network Carbonization

Circular slices were punched out of Whatman cellulose filter paper (WHA10347513, Sigma-Aldrich) and annealed at 1,100°C under argon atmosphere for 1 h (heating rate 1°C min^{-1}) using a tubular furnace (Nabertherm).

Material Characterization

The structure and morphology of the carbon network (CNW) were investigated by means of X-ray diffraction (XRD, Bruker D8 Advance diffractometer with CuK$_\alpha$ radiation) and scanning electron microscopy (SEM, Zeiss Auriga). N$_2$ adsorption-desorption isotherms were determined and analyzed by means of an Autosorb-iQ (Quantachrome). Raman measurements were performed using a confocal InVia Raman micro spectrometer with a 633 nm laser (Renishaw; each spectrum was taken as the average of three 10-s accumulations). The morphology of the CNW and cycled electrodes was investigated using high-resolution scanning electron microscopy (LEO 1550VP Field Emission SEM, Zeiss). The SEM (ZEISS Auriga) is equipped with an EDS detector (INCAPentaFETx3, Oxford Instruments), which was used for energy-dispersive X-ray spectrometry (EDX) analysis at an acceleration voltage of 15 kV. The cycled electrodes were transferred in an in-house designed transfer box under argon atmosphere into the SEM antechamber without being exposed to air.

Electrochemical Characterization

Three-electrode Swagelok cells were assembled in an argon-filled glove box for the electrochemical characterization. All potential values given in this manuscript refer to the Li/Li$^+$ quasi-reference electrode. Whatman glass fiber GF/D disks (thickness: ca. 0.67 mm) were used as separator. 1 M LiPF$_6$ in a 1:1 volume mixture of ethylene carbonate (EC) and dimethyl carbonate (DMC; premixed by UBE) was used as organic electrolyte. Alternatively, LiTFSI (3M) and Pyr$_{14}$TFSI [synthesized following the description reported by Kim et al. (2012)] were mixed in a 2:8 molar ratio and used as ionic liquid-based electrolyte. Symmetric cells were galvanostatically cycled using a battery cycler (S4000, Maccor Inc.). Cut-off potentials of ±0.5 V vs. the Li reference electrode (Honjo; 500 μm) were used for both working and counter electrode. Electrochemical impedance spectroscopy (EIS) was performed to monitor the interfacial resistance as a function of time. Frequencies ranging from 10 mHz to 200 kHz and a voltage amplitude of 10 mV were applied using a VMP (BioLogic). All electrochemical tests were performed in climatic chambers at 20°C (ΔT = ±1°C; Binder).

RESULTS AND DISCUSSION

Preparation and Characterization of 3D Carbon Network (CNW)

The physical characterization of the (filter) paper derived CNW is illustrated in **Figure 1**. Photos of the paper precursor and the carbonized free-standing 3D network are shown in **Figure 1A**. During carbonization, the paper disks shrink from a diameter of 18–12 mm with a rather uniform weight of ca. 0.1 mg. The corresponding SEM micrographs (**Figures 1B,C**) of the CNW samples reveal a homogeneous structure of interwoven carbon fibers. The nitrogen adsorption-desorption measurements of CNW (**Figure 1D**) show a Type I isotherm behavior (Sing et al., 1985), indicating the rather high microporosity accounting for a total pore volume of 0.6 cm^3 g^{-1} (inset **Figure 1D**) and BET surface area of 1,208 m^2 g^{-1}. The XRD pattern (**Figure 1E**) of the CNW does not evidence any sharp reflection, suggesting a mostly amorphous structure. The broad features at around 22° and 45° are assigned to the (002) and (101) reflections of defective graphene layers. Accordingly, the Raman spectrum (**Figure 1F**) exhibits the D (1,344 cm^{-1}) and G (1,592 cm^{-1}) bands ascribed to the defect-induced and E$_{2g}$ graphitic modes, respectively. The ID:IG ratio (0.96) indicates for a significant presence of sp^2 carbons (Ferrari and Robertson, 2000; Dou et al., 2019). Finally, the EDX analysis (**Supplementary Figure 1**) confirms that the sample is consisting of pure carbon, as no heteroatoms were detected.

Lithium Stripping/Plating Using Different Electrolytes

Figure 2A displays the plating/stripping test performed for a symmetric Li@CNW/CNW@Li cell (see cell scheme in the same figure) using a standard organic carbonate electrolyte. In the first two cycles, a relatively large amount of lithium (3.5 mAh cm^{-2}) is stripped and plated at low current (0.1 mA cm^{-2}) to establish the total lithium storage capability. The following cycles were performed at 0.5 mA cm^{-2} for 5 h, involving the plating/stripping of 2.5 mAh cm^{-2}. As seen

FIGURE 1 | Characterization of the paper-derived carbon network (CNW) material: **(A)** Photograph of the filter paper and as-prepared, free-standing CNWs; SEM images of the CNW with different magnifications, i.e., **(B)** 500x and **(C)** 1,500x; **(D)** nitrogen adsorption-desorption isotherm and pore size distribution of the CNW (inset); **(E)** XRD pattern; and **(F)** Raman spectrum of the CNW.
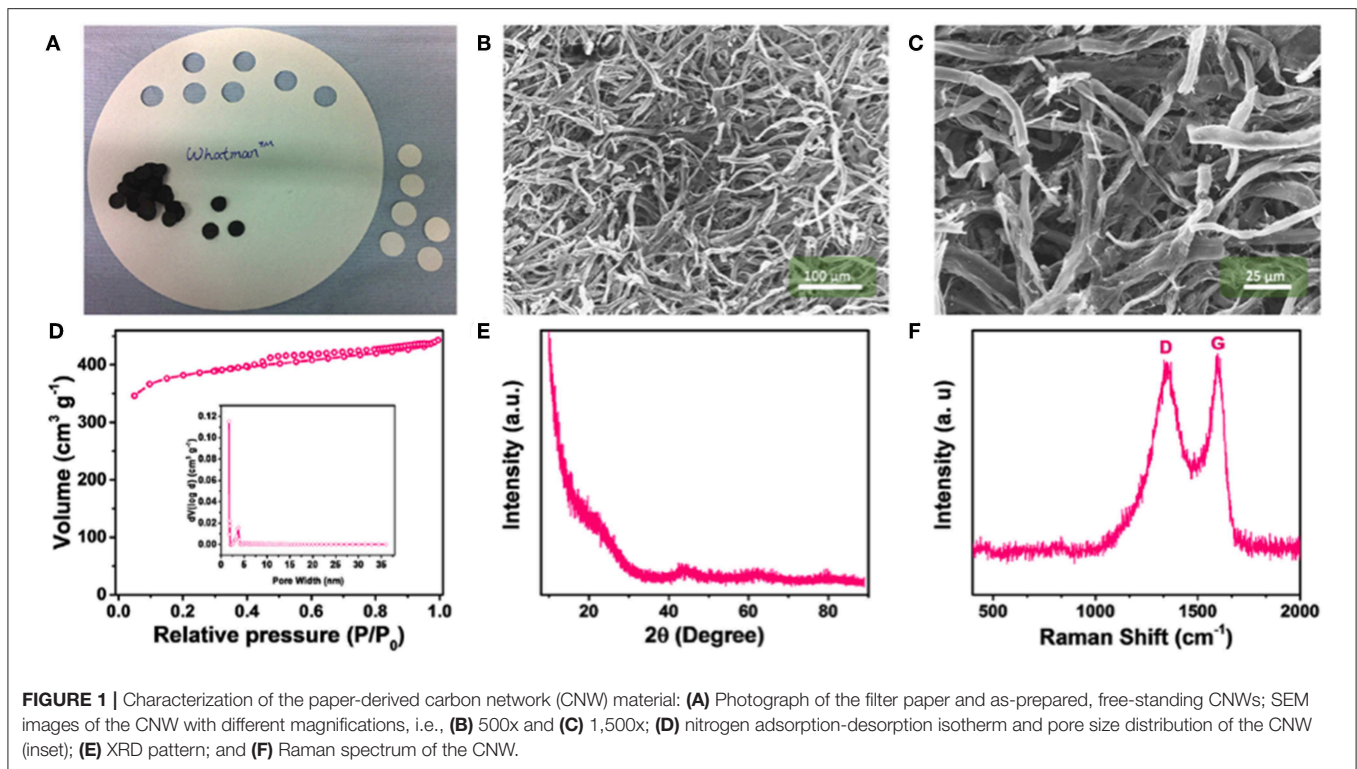
in the figure, a rather stable cycling performance is achieved for 1,600 h (i.e., 148 cycles) with a rather low overpotential (<0.1 V), though increasing upon cycling. Nonetheless, these results confirm that the very simple approach herein exploited, i.e., interlaying the conductive CNW, allows for a rather stable cycling performance of lithium metal anodes—even in organic electrolytes and for a rather large amount of lithium cycled (2.5 mA h cm^{-2}). To further optimize the system, we employed an ionic liquid-based electrolyte, which is known to allow for the highly homogeneous and reversible lithium deposition at stable overpotentials (Appetecchi et al., 2012; Grande et al., 2015; MacFarlane et al., 2016). The corresponding plating/stripping tests for a symmetrical Li@CNW/CNW@Li cell incorporating Pyr$_{14}$TFSI-LiTFSI as electrolyte is displayed in **Figure 2B**. For comparison, the performance of a cell composed of two bare Li metal electrodes, cycled under the same conditions, is also reported (**Figure 2C**). The cell with the bare Li metal electrodes shows a stable (for 10 h at least), but very high overpotential of about 0.5 V. Differently, the cell incorporating the CNW reveals a very stable overpotential—only slightly higher than 0.1 V—for more than 2,000 h. In fact, the overpotential appears much more stable than for the carbonate-based electrolyte, indicating an enhanced (electro-)chemical stability of the IL-based electrolyte which results in lower (if any) overvoltage increase.

Comparative EIS Investigation

For the further understanding of the lower overpotential resulting from the presence of the CNW, the performance of

two symmetric cells employing the same IL-based electrolyte, but with or without the interlaying CNW layers was compared. The cells were left in open circuit (OC) conditions for 7 days while electrochemical impedance measurements were taken every day to follow the evolution of the internal impedance. The results are displayed in **Figures 3A,B**. Immediately after assembly, the two symmetric cells showed similar electrode impedance values, considering the low frequency intercept of the depressed semicircle. However, upon aging, during which the spontaneous lithiation of the CNW in direct contact with the lithium electrode occurs, the two cells showed a rather opposite behavior. The impedance of the cell with two bare Li electrodes continuously increased to 430 Ω cm^2 after 1 week. In contrast, the impedance of the cell with the Li@CNW electrodes decreased to 50 Ω cm^2 after 1 day to remain stable upon further aging. In fact, following the potential of each Li@CNW electrode (using a lithium metal quasi-reference electrode) reveals that the potential drops from about 0.55–0 V vs. Li/Li$^+$ within 1 day (**Figure 3C**), indicating that the CNW is spontaneously lithiated by the lithium metal underneath without applying any current or voltage. Such lithiated CNW provides a much larger electrochemically active surface compared to the sole lithium foil, explaining the comparably lower internal impedance. Additionally, the electrode/electrolyte interface is stabilized as suggested by the stable resistance over time. To confirm this observation, we prelithiated two CNW sheets "*ex situ*" and assembled a symmetric cell with such CNWLi electrodes (**Figure 3D**). Indeed, the diameter of the semicircle is essentially the same, supporting our previous considerations.

FIGURE 2 | Room temperature (20°C) galvanostatic plating/stripping experiments for three-electrode cells composed of two **(A)** Li@CNW electrodes with the organic electrolyte at 0.5 mA cm^{-2} for 5 h (2.5 mAh cm^{-2}), **(B)** Li@CNW electrodes with the IL electrolyte at 1 mA cm^{-2} for 0.1 h (0.1 mAh cm^{-2}), and **(C)** Li metal electrodes with the IL electrolyte at 1 mA cm^{-2} for 0.1 h (0.1 mAh cm^{-2}).
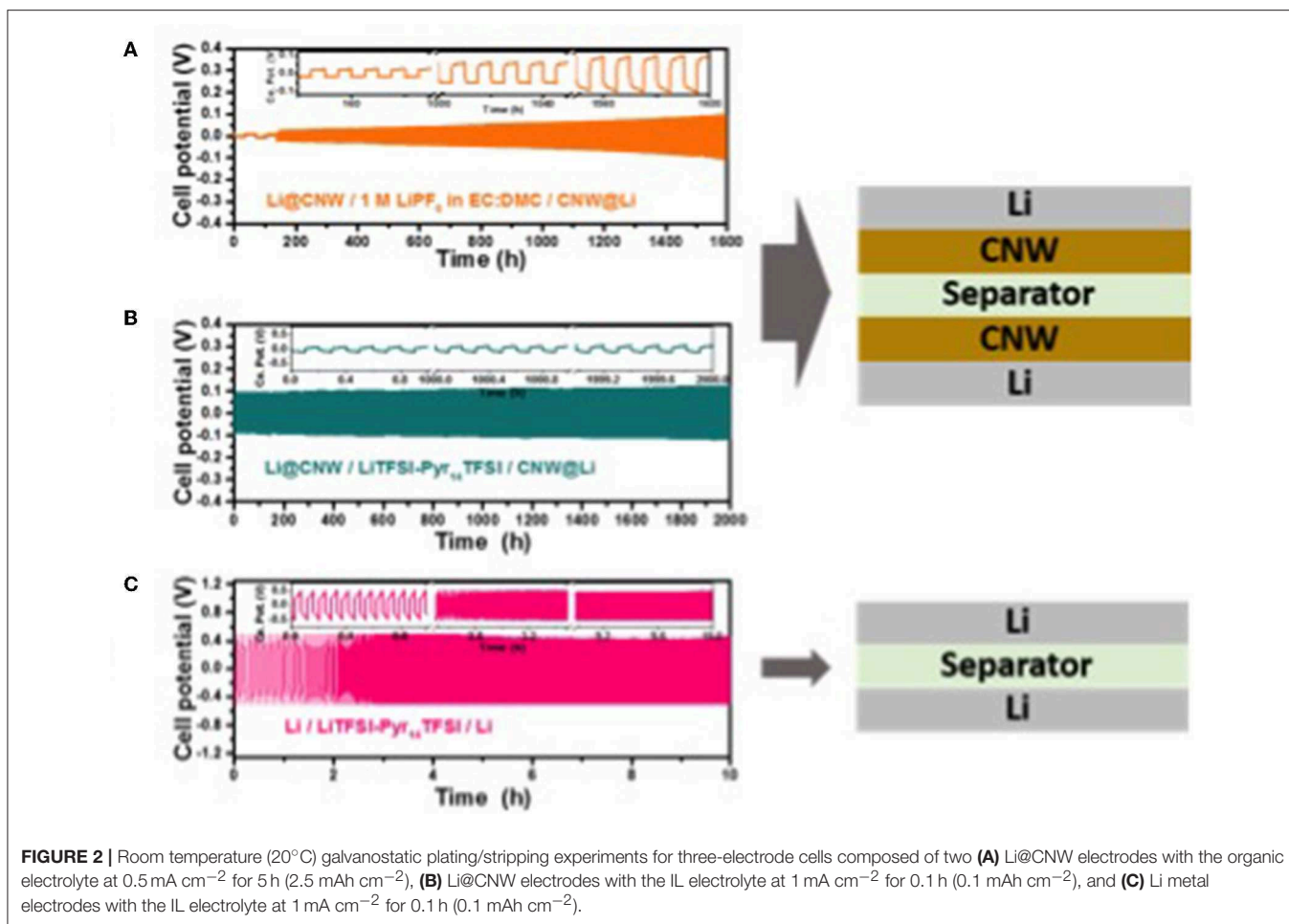
The contact resistance, however, is slightly higher, presumably due to the missing lithium layer underneath. However, effects of the prelithiation process, resulting in a very particular interface, cannot be excluded. This is also reflected in the slightly higher overpotential of the cell employing the CNWLi electrodes (CNWLi; **Supplementary Figure 2**) compared to the symmetric Li@CNW cell, suggesting that the "spontaneous" ("*in situ*") lithiation is advantageous—at least compared to the rather simple prelithiation process employed herein.

Ex situ SEM Analysis

To further elucidate the optimized performance of the Li@CNW electrodes vs. bare Li metal electrodes, SEM micrographs of cycled Li@CNW electrodes were taken, specifically of the interface between the CNW layer and the lithium metal layer (**Figure 4**). The morphology of the surface (separator side) of the cycled Li@CNW electrode is shown in **Figures 4A,B** while the surface of the Li foil underneath is displayed in **Figures 4C,D**. In fact, very different morphologies are observed. **Figures 4A,B** show that an SEI layer is formed on the topmost surface of CNW. This SEI layer, not directly being subjected to the mechanical stress of lithium metal plating and stripping, is presumably more stable than that formed on the Li metal electrode surface. Upon plating, lithium fills the void interspaces between the carbon

fibers. During the following stripping, the lithium inside the CNW interspaces is oxidized, however, leaving the SEI layer on the CNW topmost surface rather intact. A rather different morphology is observed on the surface of the underneath Li metal layer (**Figures 4C,D**), in which also a few embedded carbon fibers are observed. Mossy lithium is clearly observed on this side. Based on these observations, the following mechanism is proposed upon continuous plating/stripping cycles: Lithium metal deposits in the interspace between the carbon fibers, while the SEI formation occurs on the topmost surface of the CNW. As carbon fibers are conductive, the mossy lithium can grow on the surface and is stored between the carbon fibers. As the carbon network has a larger surface area compared to lithium metal, Li is mostly plated inside the CNW layer rather than on the Li electrode surface. The SEI formed on top (**Figure 4B**) is stabilized by the carbon network. This SEI is not subjected to the mechanical stress of a growing (upon plating) and retracting (upon stripping) Li metal surface, inducing cracking and pitting (Grande et al., 2015; Lin et al., 2017; Wood et al., 2017). Apparently, the very simple approach of applying the CNW on top of the lithium metal surface in combination with the use of an IL-based electrolyte is very effective and efficient in stabilizing the outer SEI and, thus, the lithium stripping/plating overpotential.
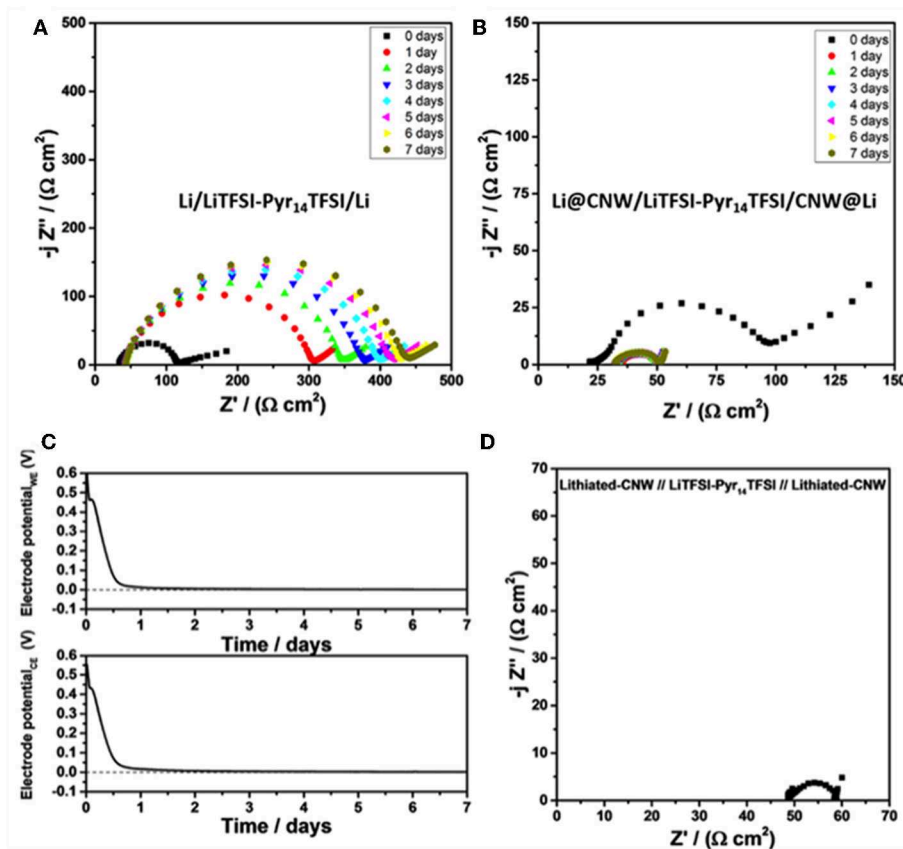
FIGURE 3 | Nyquist plots for the **(A)** Li/LiTFSI-Pyr$_{14}$TFSI/Li cell and **(B)** Li@CNW/LiTFSI-Pyr$_{14}$TFSI/CNW@Li cell upon storage in OCV conditions at 20°C. The corresponding voltage profiles for both Li@CNW electrodes in the Li@CNW/LiTFSI-Pyr$_{14}$TFSI/CNW@Li cell are shown in **(C)**; a lithium metal quasi-reference was used for this experiment. **(D)** The Nyquist plot for the CNW$_{Li}$/LiTFSI-Pyr$_{14}$TFSI/CNW$_{Li}$ cell at 20°C (the CNW electrodes were prelithiated by contact with Li metal in presence of the electrolyte to favor Li$^+$ ion mobility). Please note the different scales for the three Nyquist plots.

Critical Evaluation of the Volumetric Capacity

Nevertheless, critical remains to be the achievable volumetric energy density—at least in the present, non-optimized state due to the additional volume of the CNW interlaying layer. For a quick estimation, let us consider the volumetric capacity in the present case. The combination of the two components, i.e., the lithium metal electrode and the CNW layer, results in a total layer thickness of 0.06 cm (0.05 cm for the lithium foil and 0.01 cm for the CNW). Herein, we reported the cycling of an areal capacity for Li@CNW of 2.5 mAh cm^{-2}. Accordingly, the volumetric capacity of the Li@CNW electrode is about 41.7 mAh cm^{-3}. This first estimation, however, might be reconsidered, since the CNW provides a very high porosity, which is (partially) filled with lithium. In fact, after 100 cycles, the thickness of the Li@CNW electrode was determined to be only about 0.05 cm. Keeping in mind the given uncertainty for the thickness determination, the volumetric capacity is somewhere in the range of 41.7–50.1 mAh cm^{-3} (the latter values is calculated for a thickness of 0.05 cm). Compared to the volumetric capacity of commercial graphite anodes, however, with a specific capacity of ca. 325 mAh

g^{-1} and an electrode density of approximately 1.6 g cm^{-3} (Mao et al., 2018), i.e., ca. 520 mAh cm^{-3}, this appears rather low. To achieve a comparable volumetric capacity for the Li@CNW anode, one would need to cycle an areal capacity of ca. 26 mAh cm^{-2} (i.e., 520 mAh cm^{-3} * 0.05 cm). In the given case, this would mean that 25.2% of the total lithium (thickness: 0.05 cm, diameter: 1.2 cm) is reversibly stripped and plated if we consider the theoretical volumetric capacity of Li metal (2,061 mAh cm^{-3}). At first glance, this does not appear very much. Nonetheless, given the commonly reported values for the coulombic efficiency for lithium metal electrodes of about 99.2% (Ai, 2018), preserving a stable cycling in the long term might be challenging—or require a large excess of lithium to start with. In this case, the threshold coulombic efficiency to maintain 80% capacity retention after 1,000 cycles is calculated to be 99.83% on the full-cell level ($\sqrt{(1000\&0.8/(1+((1-25.2\%)/(25.2\%)))}$ = 0.9983), i.e., a value that appears rather ambitious. As this finally also depends on the electrochemical reactions occurring at the cathode, the next step will be a critical evaluation of the coulombic efficiency in Li@CNW-comprising full-cells.
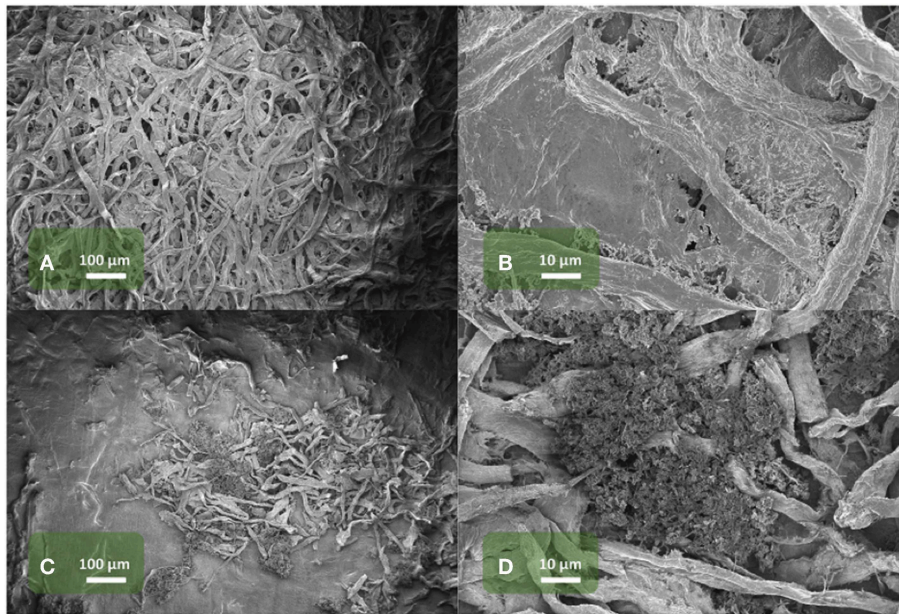
FIGURE 4 | SEM micrographs of a disassembled Li@CNW electrode, cycled in the IL-based electrolyte: The top surface of the CNW, i.e., the side which is in contact with the separator, is shown in **(A,B)** at different magnifications. The top surface of the Li foil, i.e., the side which is in contact with the CNW, is shown in **(C,D)** at different magnifications.

CONCLUSIONS

To summarize, a conductive 3D carbon network (CNW) derived from simple filter paper was used to fabricate carbon/lithium composite electrodes (Li@CNW). This CNW is spontaneously lithiated when getting in contact with the lithium metal, resulting in a substantial decrease of the impedance. Simultaneously, the highly increased surface area leads to a dramatically decreased local current density and, thus, more homogeneous lithium deposition at the macroscale, accompanied by very low and stable overpotentials when employing the ionic liquid-based electrolyte. Moreover, the porous CNW structure provides sufficient space to host large amounts of metallic lithium, thus, promising exceptionally high gravimetric specific capacities. Carefully considered, however, has to be the volumetric capacity—especially with respect to the total amount of lithium that is reversibly cycled. In fact, a brief calculation and comparison with graphite-based electrodes indicates that the advantages of lithium metal electrodes will be of commercial relevance only, if sufficiently large amounts of lithium are cycled (different from common literature reports) and this highly reversible, i.e., without significant coulombic efficiency losses.

DATA AVAILABILITY STATEMENT

The datasets generated for this study are available on reasonable request to the corresponding authors.

AUTHOR CONTRIBUTIONS

XD and MD performed the experimental work under the guidance of G-TK and SP. XG synthesized the ionic liquid-based electrolyte. XD and MD conducted the data analysis and wrote a first draft of the manuscript which was brought to its final version by DB and SP.

FUNDING

ACKNOWLEDGMENTS

SUPPLEMENTARY MATERIAL

The Supplementary Material for this article can be found online at: https://www.frontiersin.org/articles/10.3389/fmats.2019.00241/full#supplementary-material

REFERENCES

Ai, X. (2018). Heavy metal can be used as a negative electrode. Where is the road? *Energy Storage Sci. Technol.* 7, 37–39. https://caod.oriprobe.com/articles/53010841/ke_chong_jin_shu_zuo_fu_ji___lu_zai_he_fang__.htm

Appetecchi, G. B., Montanino, M., and Passerini, S. (2012). "Chapter 4: Ionic liquid-based electrolytes for high energy, safer lithium batteries," in *Ionic Liquids: Science and Applications, ACS Symposium Series, Vol.* 1117 (Washington, DC), 67–128. doi: 10.1021/bk-2012-1117.ch004

Aurbach, D., Zinigrad, E., Cohen, Y., and Teller, H. (2002). A short review of failure mechanisms of lithium metal and lithiated graphite anodes in liquid electrolyte solutions. *Solid State Ionics* 148, 405–416. doi: 10.1016/S0167-2738(02)00080-2

Ding, M. S., Koch, S. L., and Passerini, S. (2017). The effect of 1-pentylamine as solid electrolyte interphase precursor on lithium metal anodes. *Electrochim. Acta* 240, 408–414. doi: 10.1016/j.electacta.2017.04.098

Dou, X., Hasa, I., Saurel, D., Vaalma, C., Wu, L., Buchholz, D., et al. (2019). Hard carbons for sodium-ion batteries: structure, analysis, sustainability, and electrochemistry. *Mater. Today* 23, 87–104. doi: 10.1016/j.mattod.2018.12.040

Ferrari, A. C., and Robertson, J. (2000). Interpretation of Raman spectra of disordered and amorphous carbon. *Phys. Rev. B* 61:14095. doi: 10.1103/PhysRevB.61.14095

Gao, Y., Zhao, Y., Li, Y. C., Huang, Q., Mallouk, T. E., and Wang, D. (2017). Interfacial chemistry regulation via a skin-grafting strategy enables high-performance lithium-metal batteries. *J. Am. Chem. Soc.* 139, 15288–15291. doi: 10.1021/jacs.7b06437

Grande, L., Von Zamory, J., Koch, S. L., Kalhoff, J., Paillard, E., and Passerini, S. (2015). Homogeneous lithium electrodeposition with pyrrolidinium-based ionic liquid electrolytes. *ACS Appl. Mater. Interfaces* 7, 5950–5958. doi: 10.1021/acsami.5b00209

Kim, G.-T., Jeong, S. S., Xue, M.-Z., Balducci, A., Winter, M., Passerini, S., et al. (2012). Development of ionic liquid-based lithium battery prototypes. *Electrochim. Acta* 199, 239–246. doi: 10.1016/j.jpowsour.2011.10.036

Kim, H., Jeong, G., Kim, Y.-U., Kim, J.-H., Park, C.-M., and Sohn, H.-J. (2013). Metallic anodes for next generation secondary batteries. *Chem. Soc. Rev.* 42, 9011–9034. doi: 10.1039/c3cs60177c

Li, N. W., Yin, Y. X., Yang, C. P., and Guo, Y. G. (2016). An artificial solid electrolyte interphase layer for stable lithium metal anodes. *Adv. Mater.* 28, 1853–1858. doi: 10.1002/adma.201504526

Li, Q., Zhu, S., and Lu, Y. (2017). 3D porous Cu current collector/Li-metal composite anode for stable lithium-metal batteries. *Adv. Funct. Mater.* 27:1606422. doi: 10.1002/adfm.201606422

Lin, D., Liu, Y., and Cui, Y. (2017). Reviving the lithium metal anode for high-energy batteries. *Nat. Nanotechnol.* 12, 194–206. doi: 10.1038/nnano.2017.16

Liu, L., Yin, Y.-X., Li, J.-Y., Li, N.-W., Zeng, X.-X., Ye, H., et al. (2017). Free-standing hollow carbon fibers as high-capacity containers for stable lithium metal anodes. *Joule*, 1, 563–575. doi: 10.1016/j.joule.2017.06.004

Liu, S., Wang, A., Li, Q., Wu, J., Chiou, K., Huang, J., et al. (2018). Crumpled graphene balls stabilized dendrite-free lithium metal anodes. *Joule* 2, 184–193. doi: 10.1016/j.joule.2017.11.004

Lu, Z., Zhang, Z., Chen, X., Ren, F., Wang, M., Wu, S., et al. (2018). Improving Li anode performance by a porous 3D carbon paper host with plasma assisted sponge carbon coating. *Energy Storage Mater.* 11, 47–56. doi: 10.1016/j.ensm.2017.09.011

MacFarlane, D. R., Forsyth, M., Howlett, P. C., Kar, M., Passerini, S., Pringle, J. M., et al. (2016). Ionic liquids and their solid-state analogues as materials for energy generation and storage. *Nat. Rev. Mater.* 1:15005. doi: 10.1038/natrevmats.2015.5

Mao, C., Wood, M., David, L., An, S. J., Sheng, Y., Du, Z., et al. (2018). Selecting the best graphite for long-life, high-energy li-ion batteries. *J. Electrochem. Soc.* 165, A1837–A1845. doi: 10.1149/2.1111809jes

Sing, K. S. W., Everett, D. H., Haul, R. A. W., Moscou, L., Pierotti, R. A., Rouquérol, J., et al. (1985). Reporting physisorption data for gas/solid systems with special reference to the determination of surface area and porosity. *Pure Appl. Chem.* 57, 603–619. doi: 10.1351/pac198557040603

Wood, K. N., Noked, M., and Dasgupta, N. P. (2017). Lithium metal anodes: toward an improved understanding of coupled morphological, electrochemical, and mechanical behavior. *ACS Energy Lett.* 2, 664–672. doi: 10.1021/acsenergylett.6b00650

Wu, S., Zhang, Z., Lan, M., Yang, S., Cheng, J., Cai, J., et al. (2018). Lithiophilic Cu-CuO-Ni hybrid structure: advanced current collectors toward stable lithium metal anodes. *Adv. Mater.* 30:1705830. doi: 10.1002/adma.201705830

Xu, K. (2004). Nonaqueous liquid electrolytes for lithium-based rechargeable batteries. *Chem. Rev.* 104, 4303–4418. doi: 10.1021/cr030203g

Xu, W., Wang, J., Ding, F., Chen, X., Nasybulin, E., Zhang, Y., et al. (2014). Lithium metal anodes for rechargeable batteries. *Energy Environ. Sci.* 7, 513–537. doi: 10.1039/C3EE40795K

Yang, C., Yin, Y., Zhang, S., Li, N., and Guo, Y. (2015). Accommodating lithium into 3D current collectors with a submicron skeleton towards long-life lithium metal anodes. *Nat. Commun.* 6:8058. doi: 10.1038/ncomms9058

Zhang, R., Cheng, X., Zhao, C., Peng, H., Shi, J., Huang, J., et al. (2016). Conductive nanostructured scaffolds render low local current density to inhibit lithium dendrite growth. *Adv. Mater.* 28, 2155–2162. doi: 10.1002/adma.201504117